



Buckling Safety Assessment for the Multi-Axle Steering Linkage of an 8x8 Special Purpose Vehicle

Mehmet Murat Topaç^{1*}, Merve Karaca², Aziz Başdemir¹, Batuhan Kuleli³

¹ Department of Mechanical Engineering, Dokuz Eylül University, 35397, Buca, Izmir, Turkey.

² The Graduate School of Natural and Applied Sciences, Dokuz Eylül University, 35397, Buca, Izmir, Turkey

³ Volkan Fire Fighting Vehicles, R&D Center, 35860, Torbalı, Izmir, Turkey

*murat.topac@deu.edu.tr

Received: 17 January 2019

Accepted: 12 December 2019

DOI: 10.18466/cbayarfbe.514068

Abstract

Vehicle steering mechanisms are generally considered as safety sub-systems due to their control and stability functions. Therefore, structural elements of a steering linkage should strictly resist the service loads without any overload failure. This paper reports an exemplary case study on the buckling evaluation of the multi-axle steering linkage tie rods which will be used in an 8x8 special purpose vehicle. In the first part of the study, full multibody dynamics (MBD) model of the vehicle including the steering linkage was composed by using Adams/Car™ commercial software. With this model, handling simulations were carried out to determine the service loads for various driving conditions. In order to verify the MBD model, reaction forces occur at the linkage joints were also calculated by using detailed finite element (FE) model of the entire system for the same driving conditions. In the final part of the work, buckling safety of the tie rods was assessed for the critical load case. In this way suitability of the system was evaluated in terms of buckling.

Keywords: 8x8 vehicle, multi-axle steering, multibody dynamics (MBD), simulation, finite element analysis (FEA), computer-aided engineering (CAE).

1. Introduction

Double front axle steering is a key design solution for most of the heavy-duty vehicles due to the legal axle load limits [1]. With the use of these systems, more balanced front/rear load distribution on the chassis can also be obtained. An important number of heavy duty vehicles use sophisticated double front axle steering mechanisms to provide proper turning angles of the steer axle wheels simultaneously [2, 3]. These systems should satisfy the reliability conditions under various load conditions, as well as obtaining the correct steering of the vehicle [4].

In the scope of this paper, an exemplary case study on the buckling safety assessment of the tie rods which will be used in a double front axle steering system of a new generation 8x8 ARFF vehicle is summarized. General views of the vehicle are seen in Fig.1. Ackermann steering of the vehicle is also given in Fig.2.a [5, 6]. Coordinated turning motion of the wheels (1, 2, 5 and 6)

of axle I and axle II are supplied by means of a double front axle steering linkage shown in Fig.2.b. Here, steering torque input is applied to a central idler arm (11) via a pitman arm (9) which is mounted to the output shaft of the steering box (10). Idler arm distributes the steering torque into the axle I and II employing the tie rods a, b and f. Moreover, relay lever (12) also delivers the steering torque to the wheels 2 and 6 via tie rods c and d. Detail view of the existing system can also be seen in Fig.2. Steering of the wheels 4 and 8 (axle IV) is provided through a hydraulic driven Ackermann mechanism.

Since they operate in the steering system as two force members, tie rods are subjected to axial loads. During the service, as a result of the compression forces acting along their longitudinal axes, rods can be subjected to an unstable bending also known as buckling. Because of their critical function in the steering linkage, it is crucial to satisfy the buckling strength conditions for a tie rod.



Figure 1. The 8x8 ARFF vehicle (Courtesy of Volkan Fire Fighting Vehicles, R&D division).

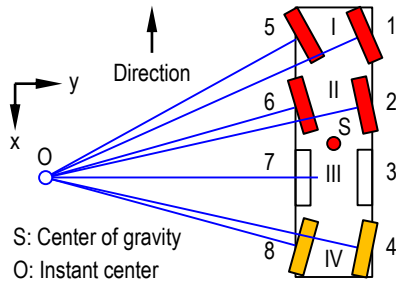


Figure 2. Ackermann steering of the vehicle [6].

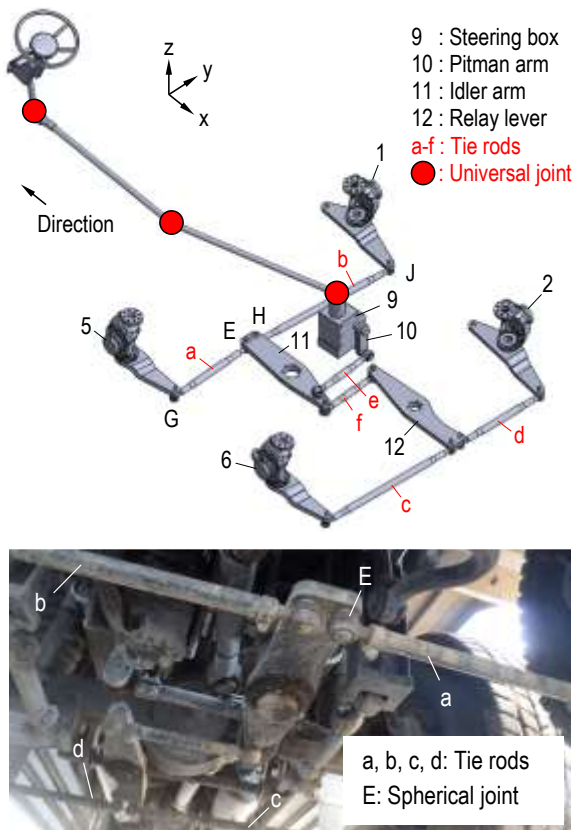


Figure 3. Double front axle steering linkage.

In order to determine the structural relevance of the tie rods used in this linkage in terms of buckling, firstly, maximum compressive service loads acting on the spherical –or ball joints of the rods a-d were determined by means of a detailed multibody dynamics (MBD) model of the ARFF vehicle. Results obtained

from this model were also verified with the use of the finite element model of the entire steering linkage. In the final part, buckling tendency of the rods was evaluated by using the design geometry and material properties of the tie rods.

2. Materials and Methods

Structure of the tie rod b is given in Fig.4 as an example. As can be seen from the cutaway view y-y, body of the component consists of a hollow cross-sectional tube has an outer diameter of D and an inner diameter of d. l is the effective length between the centers of the ball joints H and J.

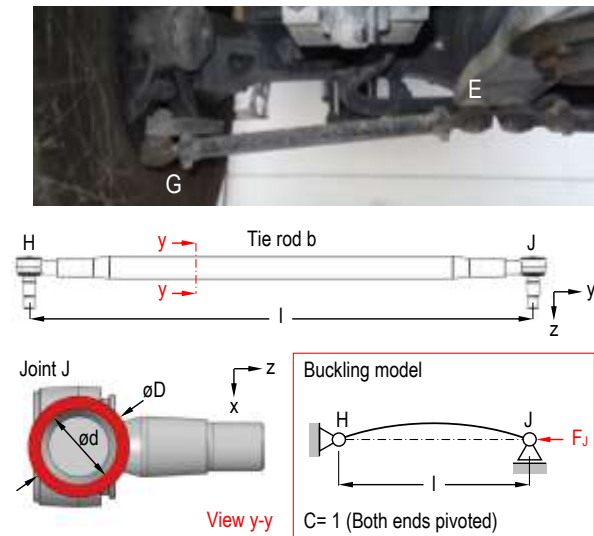


Figure 4. Tie rod structure and the simple buckling model.

As known from the literature, the Euler and the Johnson formulae are frequently used to determine the buckling behavior of the mechanical elements whose lengths are much greater than their cross-sectional areas. By using the critical load for buckling P_{cr} , the length l, the cross-sectional area A, and the modulus of elasticity of the component material E, the Euler column formula can be expressed as:

$$\frac{P_{cr}}{A} = \frac{C\pi^2 E}{\left(\frac{l}{k}\right)^2} \quad (2.1)$$

C is the end-condition constant which can be assumed as 1 for the rounded-end (or pivoted-end) parts like automotive tie rods analyzed in this study. (l/k) is named as the slenderness ratio λ . The radius of gyration k can be written as:

$$k = \left(\frac{I}{A}\right)^{0.5} \quad (2.2)$$

Here, I is the moment of inertia. By utilizing Eq. (2.1), Euler's curve can be plotted as seen in Fig.5 [7].

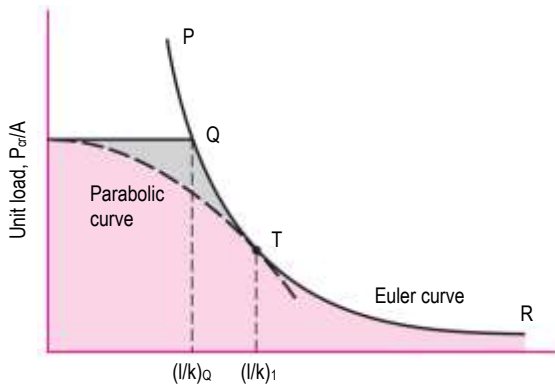


Figure 5. Euler's curve plotted using Eq. (2.1) [7].

By taking the yield point of the material S_y into account, point T is generally selected by the designers where $P_{cr}/A = S_y/2$. The corresponding value of $(l/k)_1$ can also be found as:

$$\left(\frac{l}{k}\right)_1 = \left(\frac{2\pi^2 CE}{S_y}\right)^{0.5} \quad (2.3)$$

As an alternative of Euler formula, the Johnson (or parabolic) equation is generally preferred in the design process of automotive parts. By using Eq. (2.3), Johnson formula can also be written as:

$$\frac{P_{cr}}{A} = S_y - \left(\frac{S_y l}{2\pi k}\right)^2 \frac{1}{CE} \quad (2.4)$$

The slenderness ratio λ is the characteristic factor in deciding whether the Euler formula or the Johnson formula is used for the buckling assessments. If the slenderness ratio is greater than the value which is obtained from Eq. (2.3), Johnson formula is generally utilized for buckling assessments [7].

3. Results and Discussion

3.1 Multibody Dynamics Model of the Vehicle

In order to predict the critical compressive load on the tie rods during the service, firstly, a detailed multibody dynamics (MBD) model of the ARFF vehicle was built by using Adams/Car™ commercial software as shown in Fig.6.a. In this model, all of the linkage elements (Fig.6.b) are assumed to be rigid. The model consists of six major subsystems: pneumatic tires, suspension and steering linkages, vehicle body, powertrain, and brake system. By using this model, selected driving maneuvers namely, zero-speed steering, lane change, ramp steer, J-turn, and braking at a deceleration of 0.6 g were carried out. Road profile of the National Fire Protection Association (NFPA) lane change maneuver [8] and superimposed graphical view of the simulation for the full laden vehicle at a constant velocity of $v_F=40$ km/h are given in Fig.6.c and Fig.6.d respectively.

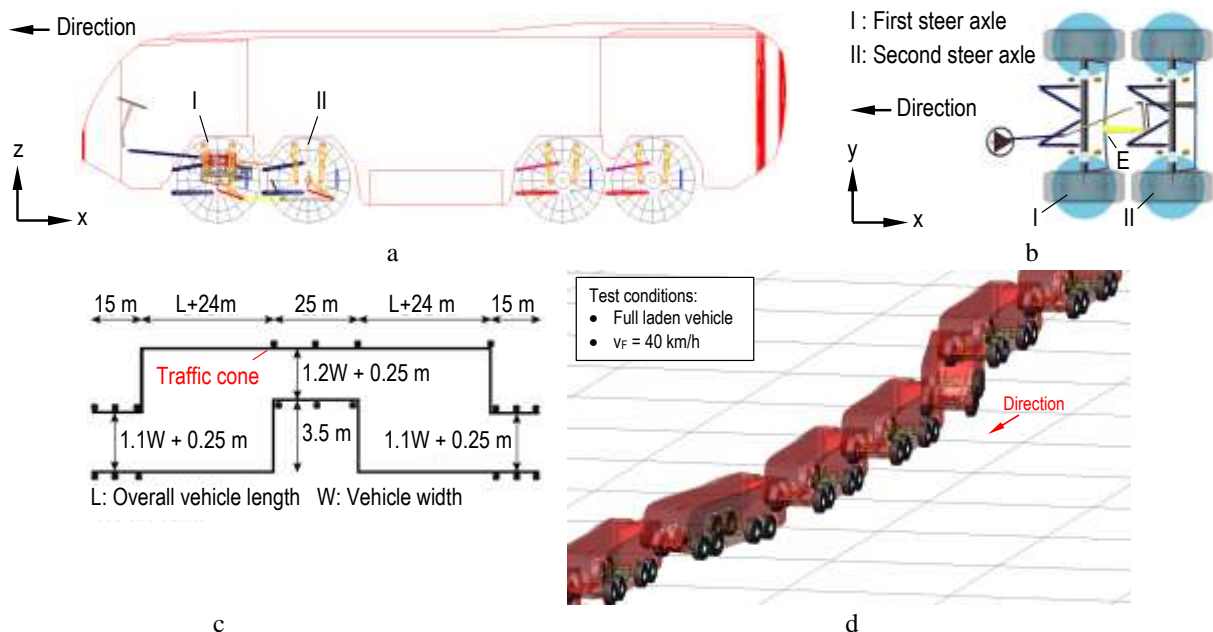


Figure 6.a. Full vehicle model **b.** MBD model of the steering linkage **c.** Standard road profile for lane change maneuver according to [8] **d.** MBD simulation of the lane change maneuver.

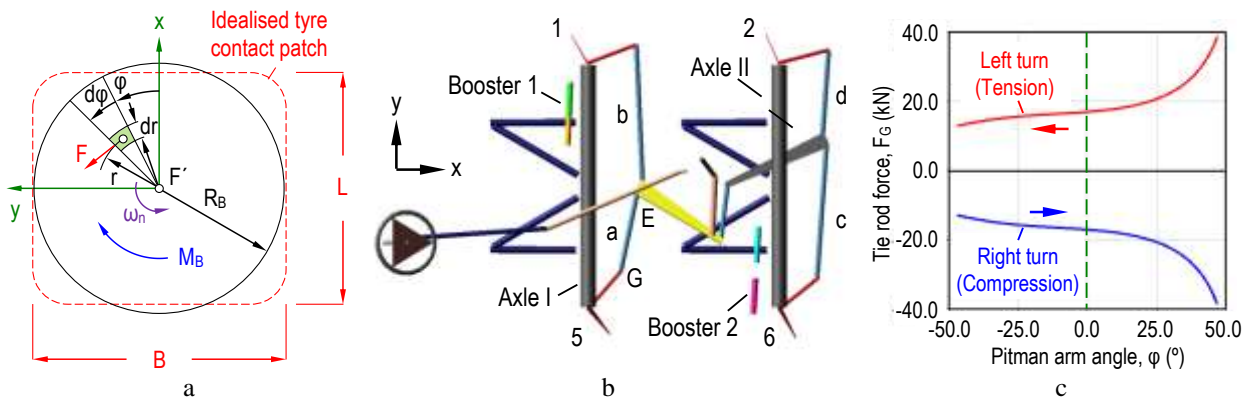


Figure 7. a. Idealized tyre contact patch [10] b. Steering simulation of the linkage c. Reaction force variation at the joint G for the zero-speed steering case [6].

In order to simulate the zero speed steering effect on the steering linkage, maximum reaction moment M_B at the tyre contact patch was obtained by utilizing “the bore torque approach” [9,10]. M_B can be calculated as:

$$M_{Bmax} = \frac{1}{A} F \int_A r dA \quad (2.5)$$

Here, F is the unit friction force which can be achieved by using the vertical wheel load P and tire-road friction coefficient μ . Contact patch area A can be obtained from the idealized tyre contact patch model given in Fig.7.a [9-11]. Hence, M_B can be easily expressed as:

$$M_{Bmax} = \frac{1}{R_B \pi} F \int_0^{R_B} \int_0^{2\pi} r r d\phi dr = \frac{2}{3} R_B F \quad (2.6)$$

Results of the MBD simulations indicated that compressive forces acting on the rods can be raised to a maximum value about 40 kN for the zero-speed steering maneuver which is the highest value obtained among the selected driving cases. Resultant reaction force variation at the spherical joint G (Fig.6.b) that corresponds to the maximum turning range of the wheel 5 (or pitman arm) for the stationary condition of the vehicle is seen in Fig.7.c as an example [6].

3.2 Finite Element Analysis of the Linkage

In order to verify the reaction force results obtained from the MBD simulation, finite element (FE) model of the entire linkage was also built via ANSYS® Workbench™ commercial software package. Joints used in this model and load model for the zero speed steering case are shown in Fig.8 and Fig.9 respectively. In Fig.8, initials A-G represent the forces, moments –or bore torques and the boundary conditions used in the model. Here, forces (Force 1 and Force 2) which are generated by the booster cylinders used in axle I and axle II were also taken into account. In order to obtain force-moment balance, fixed support boundary condition was used at the pitman arm-steering box

connection. To build the FE model, SOLID187 which is a higher order 3-D, 10-node element was utilized. SOLID187 has quadratic displacement behavior and is well suited to modeling irregular meshes [12].

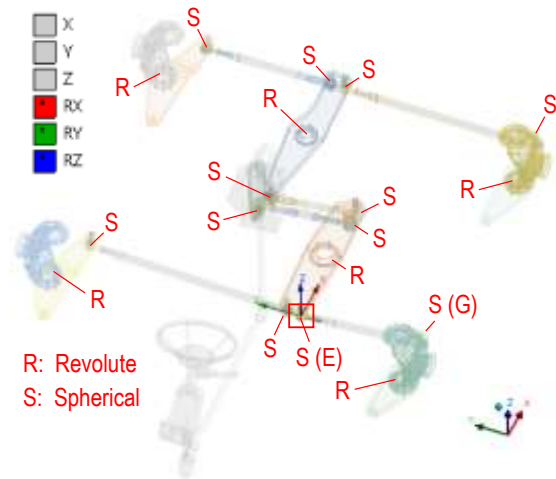


Figure 8. FE model structure.

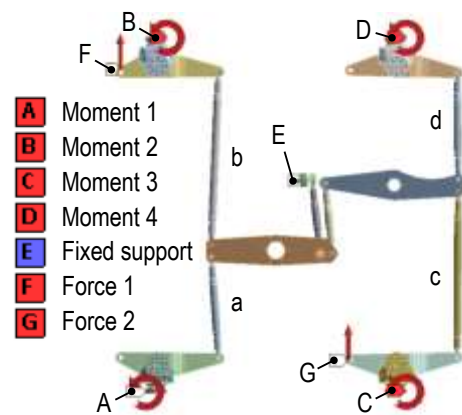


Figure 9. Load model and the mesh structure.

Basic mechanical properties of the tie rod material used in the FE analyses are given in Table 1. Here, ρ is the

mass density and ν is the Poisson's ratio. FE model consists of 395,546 nodes and 227,140 elements. Fig. 10 illustrates the mesh structure. Equivalent (von Mises) stress distribution on the linkage components for this case is also seen in Fig. 11.

Table 1. Basic mechanical properties of tie rod material.

ρ (kg/m ³)	E (GPa)	ν (-)	S _y (MPa)
7850	200	0.3	355

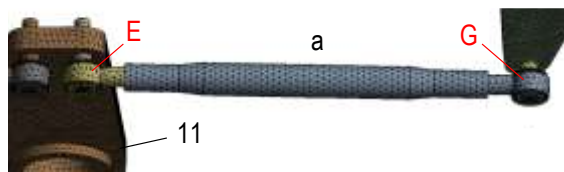


Figure 10. Mesh structure.

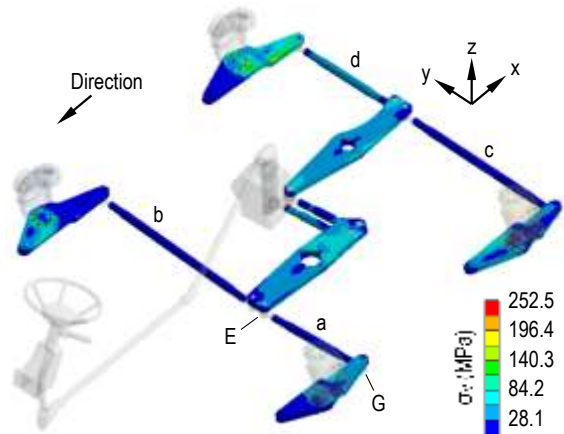


Figure 11. Equivalent stress distribution on the full steering mechanism.

Results of this analysis indicated that deviation of the joint force values obtained from MBD and FE models does not exceed about 3%.

3.3 Buckling Safety Assessment

In order to illustrate the generalized possible design region for the tie rods where the buckling failure does not occur, Euler's curve was plotted for a range of S_y which represents various material types. Data sets for each S_y value were generated and utilized to construct a 3-D surface in MATLAB® environment as seen in Fig.12. To satisfy the safety requirements in terms of buckling, the point which represents the design properties of a tie rod should be within the volume under the surface. Euler's curve plotted for the current tie rod material is also seen in Fig.13. Design properties of the longer tie rods (b and c) used in the existing linkage are also given as example in Table 2.

Table 2. Some design properties for tie rods b and c.

D/d (-)	A (mm ²)	I (mm ⁴)	l (mm)
1.3	829.4	204,442.3	1033

Possible crookedness of the rods was neglected for buckling assessments. Due to the structural dimensions, (l/k) and (l/k)₁ values were calculated as 65.79 and 105.45 respectively. Since the following condition is satisfied for the components, Johnson parabola was utilized for buckling evaluation:

$$\left(\frac{l}{k}\right) \leq \left(\frac{l}{k}\right)_1 \quad (3.1)$$

End-condition constant C was assumed as 1 according to the simple buckling model given in Fig 4. The extreme value of the P_{cr} was chosen as 40 kN according to Fig.7.b.

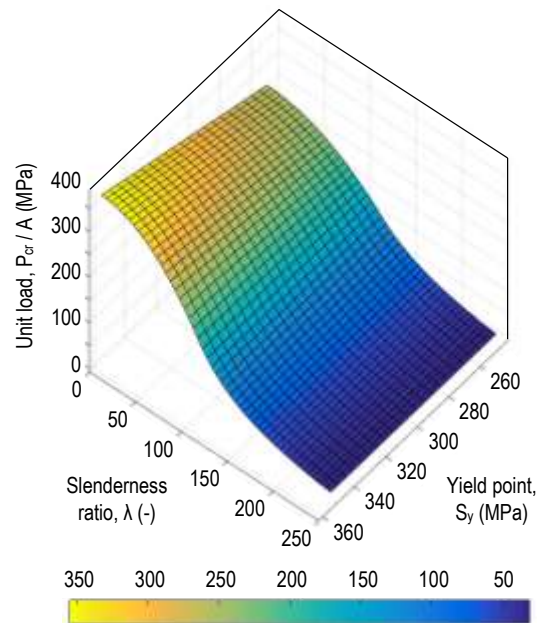


Figure 12. Euler's curve-based design chart as functions of the S_y and λ .

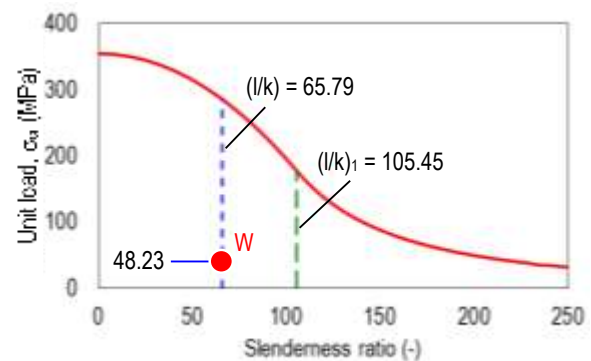


Figure 13. Euler's curve for S_y= 355 MPa and the data given in Table 2.

In literature, recommended range for buckling factor of safety n_b is 1.7 to 3.5 [13]. By utilizing Eq. (2.4) and the data given in Table 1, required P_{cr}/A value was calculated as 286 N/mm^2 which is about 5.93 times greater than the unit load obtained for rod b and rod c of the existing linkage. In other words, the minimum n_b value for the tie rods of the entire linkage was obtained as 5.93 for the most critical case. Design point for tie rods b and c is illustrated as the point “W” in Fig.13.

3.4 Mass Reduction

Results indicated that mass reduction is possible for tie rods due to their high factor of safety. By using the notation given in chapter 2, D/d ratio was obtained as 1.21 for the maximum factor of safety value of $n_b = 3.5$.

Here, the inner diameter “d” which also represents the diameter of the tie rod mounting screw of the spherical joint was assumed as constant. For this condition, wall thickness of the rod tubes is about 33% lower than the initial ones. As a result, the mass of the components can be reduced about 22%. In order to determine the effect of this design alteration on the strength properties, FE analyses were also repeated for tensile and compressive loading modes by utilizing $P_{cr} = 40 \text{ kN}$. Von Mises stress distributions for $D/d = 1.3$ which represent the original design and $D/d = 1.21$ are compared in Fig.14. According to the numerical results, the maximum value of the equivalent stress does not exceed $\sigma_{Vmax} = 109 \text{ MPa}$ as seen in the figure. Hence, it can be concluded that safety condition is also satisfied for the latter case ($D/d = 1.21$).

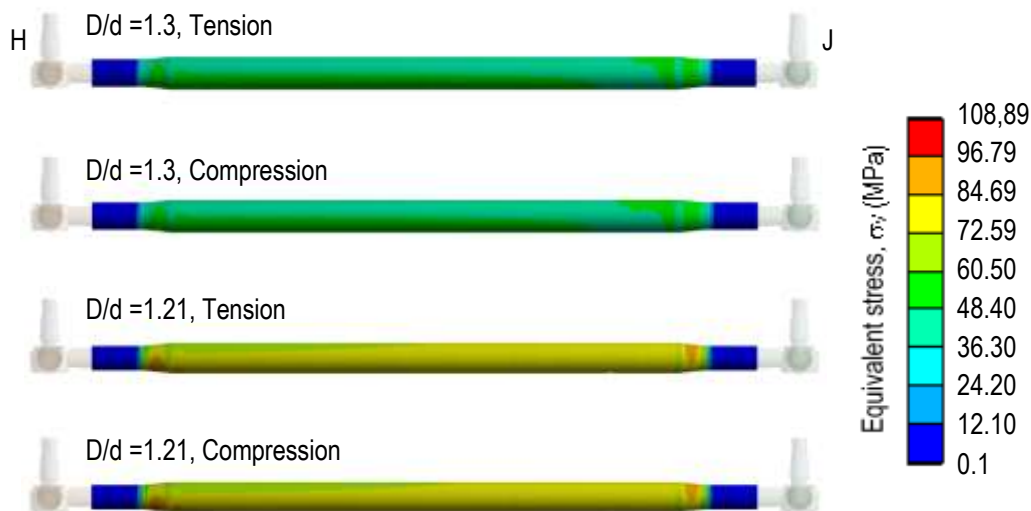


Figure 14. Comparison of the von Mises stress distributions for various D/d ratios.

4. Conclusion

In this work, a numerical case study on the buckling safety assessment of the tie rods used in the double front axle steering mechanism of an 8x8 ARFF was summarized. The evaluation was carried out by using a method including the multibody dynamics (MBD) and finite element (FE) analysis. In order to determine the critical compressive service loads on the tie rods, a detailed MBD model of the vehicle was composed. Selected maneuvers were simulated by utilizing this model. In order to verify the reaction force values obtained from the MBD model, FE analyses of the entire steering linkage were also achieved. Results of this analysis indicated that deviation of the joint force values obtained from MBD and FE models does not exceed about 3%. Buckling safety assessments also showed that the critical compressive load P_{cr} which was calculated by using Johnson formula is greater than the axial compressive tie rod forces for the zero-speed steering maneuver. Minimum buckling factor of safety is greater than the limit value given in the literature. It

was concluded that tie rods used in this mechanism satisfy the safety conditions for the critical load conditions in terms of buckling. Results of this study also indicated that it is possible to reduce the mass of the tie rods about 22% while preserving the safety conditions.

Acknowledgment

This study was supported by Volkan Fire Fighting Vehicles, Izmir, Turkey. Authors are also grateful for the licensed software support of BİAS Mühendislik Ltd. Şti. Modeling and analyses given in Chapters 3.1 and 3.2 were carried out by the first and the second author as a part of an R&D project (project no: 3170127) supported by The Scientific and Technological Research Council of Turkey (TÜBİTAK).

Ethics

There are no ethical issues after the publication of this manuscript.



References

1. Wu, J, Zhang, S, Yang, Q. Deformation Effect Simulation and Optimization for Double Front Axle Steering Mechanism, 4th International Conference on Computer Modeling and Simulation, Hong Kong, China, 2012, pp 27-31.
2. Matschinsky, W, Radführungen der Straßenfahrzeuge; Springer-Verlag: Berlin, Germany, 2007; pp 265.
3. Watanabe, K, Yamankawa, J, Tanaka, M., Sasaki, T., Turning characteristics of multi-axle vehicles, *Journal of Terramechanics*, 2007, 44, 81-87.
4. Yucheng, L, Wei, Z, Guifan, Z, Cong, W, Kinematical models and emulation of multi-axle steering of off-highway vehicles with multi-axle, *Journal of Commercial Vehicles*, 1995, 104, 261-267.
5. Topaç, M.M, Kaplan, A., Kuleli, B, Deryal, U. Design of a Multi-Axle Steering Mechanism for a Special Purpose Vehicle: Kinematic Design and Optimization, book of full text proceedings of 8th International Advanced Technologies Symposium, Elazığ, Turkey, 2017, pp 502-509.
6. Topaç, M.M, Karaca, M, Kuleli, B. A Design Optimization Study for the Multi-Axle Steering System of an 8x8 ARFF Vehicle, Proceedings of the 3rd International Conference on Applied Physics, System Science and Computers, Dubrovnik, Croatia, 2018, pp 342-347.
7. Shigley, J.E, Mischke, C.R, Mechanical Engineering Design; McGraw-Hill, Inc.: New York, U.S.A, 1989; pp 123.
8. Kann, D.F, McDonald, J.W. NFPA® 414: Standard for Aircraft Rescue and Fire-Fighting Vehicles 2017 Edition; National Fire Protection Association: Massachusetts, U.S.A, 2017; pp 414-40.
9. Sharp, R.S, Granger, R, On car steering torques at parking speeds, *Proceedings of the Institution of Mechanical Engineers, Part D: Journal of Automobile Engineering*, 2003, 217(2), 87-96.
10. Rill, G, Vehicle Dynamics: Lecture Notes; Fachhochschule Regensburg; Regensburg, Germany, 2006; pp 39, 40.
11. Topaç, M.M, Karaca, M, Atak, M, Deryal, U, Response surface-based design study of a relay lever for a bus independent suspension steering mechanism, *International Journal of Automotive Engineering and Technologies*, 2017, 6(Special issue 1), 1-10.
12. ANSYS Theory Reference, ANSYS Release 10.0; ANSYS, Inc.: Canonsburg, U.S.A., 2005; pp --.
13. Timoshenko S.P, Strength of Materials Part I Elementary Theory and Problems, 2nd edn; D. Van Nostrand Company, Inc.: New York, U.S.A., 1940; pp 252.